Noncontact Measurement of Autonomic Nervous System Activities Based on Heart Rate Variability Using Ultra-Wideband Array Radar

Takuya Sakamoto, *Senior Member, IEEE*, and Kosuke Yamashita

***Abstract*—The noncontact measurement of vital signs using ultra-wideband radar has been attracting increasing attention because it can unobtrusively provide information about the physical and mental condition of people. In particular, the continuous measurement of a person's time-varying instantaneous heart rate can estimate the activity level of the autonomic nervous system without the person wearing any sensors. Continuous heart rate measurement using radar is, however, a difficult task because accuracy is compromised by numerous factors, such as the posture and motion of the target person. In this study, we introduce techniques for increasing the accuracy and reliability of the noncontact measurement of heart rate variability. We demonstrate the performance of the proposed techniques by applying them to radar measurement data from a sleeping person, and we also compare its accuracy with electrocardiogram data.**

***Index Terms*—Array signal processing, biomedical monitoring, physiology, radar measurements, sensor systems and applications.**

I. Introduction

THE importance of heart rate variability (HRV) has been widely recognized in healthcare and medical applications. Pagani *et al.* [1] and Malliani *et al.* [2] conducted pioneering studies in this field, and suggested the use of the low-frequency (LF)/high-frequency (HF) ratio of HRV, which is the power ratio of the LF (0.04–0.15 Hz) to the HF (0.15–0.4 Hz) components of the HRV time series, as a convenient marker for sympathetic and vagal activity balance. This implies that sympathovagal interaction modulates cardiovascular function, and thus, early signs of various illnesses, such as diabetes, hypertension, congestive heart failure, and ischemic heart disease, can be detected using the LF/HF ratio measurement [2], whose details are reviewed in [3].

Manuscript received July 20, 2019; revised September 23, 2019; accepted October 17, 2019. Date of publication October 22, 2019; date of current version August 21, 2020. This work was supported in part by JSPS KAKENHI under Grants 15K18077, 15KK0243, and 19H02155, in part by the Japan Science and Technology Agency PRESTO under Grant JPMJPR1873, and in part by the JST COI Program under Grant JPMJCE1307. This article was presented in part at the IEEE International Microwave Biomedical Conference, Nanjing, China, May 2019. *(Corresponding author: Takuya Sakamoto.)*

T. Sakamoto is with the Graduate School of Engineering, Kyoto University, Kyoto 615-8510, Japan, and also with Japan Science and Technology Agency, PRESTO, Kawaguchi 332-0012, Japan (e-mail: sakamoto.takuya.8n@kyoto-u.ac.jp).

K. Yamashita was with the Graduate School of Engineering, University of Hyogo, Himeji 671-2280, Japan. He is now with Denso Ten Ltd., Kobe 652-8510, Japan (e-mail: kouske1995@gmail.com).

Digital Object Identifier 10.1109/JERM.2019.2948827

The advantage of using the LF/HF ratio is that it is an easy and non-invasive measurement, yet sufficiently informative to detect various clinical signs. Because of this advantage, numerous studies have been published in this field, with most studies based on contact sensors, such as electrocardiography (ECG) and photoplethysmography [4]–[8]. These studies focused on various aspects of HRV: Stanley *et al.* proposed a statistical model [4], Mateo and Laguna proposed a signal processing technique [5], Garcia-Gonzalez and Pallas-Areny proposed a new HRV index [6], and Leor-Librach *et al.* [7] proposed a mathematical model of the LF HRV. Sarkar and Koehler [8] reported on HRV as a marker of heart failure.

Studies on the LF/HF ratio have also been conducted for sleep monitoring [9]–[11]. Ako *et al.* [9] studied the relationship between HRV and electroencephalogram (EEG) recordings, and found that deep sleep suppresses sympathetic nervous activities, which is indicated by a decrease in the LF of HRV, which can be used in psychiatric disorder research. Knorr *et al.* [10] and Mellman *et al.* [11] studied respiration, ECG, EEG, electromyography, and electrooculography during sleep for injured patients. They found that, during rapid eye movement (REM) sleep, the LF/HF ratio is higher for a group that is developing posttraumatic stress disorder (PTSD) than a control group of injured patients without PTSD. Kishi *et al.* [12] studied the characteristic sleep stage transition of chronic fatigue syndrome patients.

Limitations of the LF/HF ratio have also been reported: Milicević [13] found that sympathovagal balance could not be accurately measured using the LF/HF ratio for cardiac patients, and Billman [14] indicated various issues regarding the use of the LF/HF ratio including its ambiguity. The ambiguity issue was addressed by Rosenberg *et al.* [15] and two-dimensional LF and HF scatter diagrams were proposed instead of the LF/HF ratio for discriminating various nerve activity balances. Based on these careful studies, HRV has been increasingly used in a wide range of applications [16]–[18]. Zhu *et al.* [16] used HRV to detect autonomic nervous system dysfunction related to cardiac mortality. Nardelli *et al.* [17] proposed an HRV-based emotion estimation technique. Tobón *et al.* [18] proposed a signal processing technique for the accurate estimation of HRV using ECG signals.

Recently, a number of studies have been published on noncontact heart rate and HRV measurement using a radar system instead of conventional contact sensors [19]–[23]. Hu *et al.* [19] reported an accurate signal processing technique

This work is licensed under a Creative Commons Attribution 4.0 License. For more information, see http://creativecommons.org/licenses/by/4.0/

for the noncontact measurement of heart rate using radar. Nagae and Mase [20] estimated HRV using radar data based on a template-based method and maximum entropy algorithm. Nostrati and Tavassolian [21] measured HRV using 2.4-GHz radar with an error of 2%. Mogi and Ohtsuki [22] proposed a radar-based HRV estimation method using the Viterbi algorithm. Li and Lin [23] proposed a method to estimate heart rate based on the wavelet transform and achieved an error of 3.5%. These radar-based noncontact measurement techniques have also been applied to sleep monitoring [24]–[28]. Baboli *et al.* [24] integrated 2.4-GHz radar with a commercial sleep monitoring system. Lin *et al.* [25] proposed a radar-based noncontact sleep monitoring system using manually selected signal features. Zhang *et al.* [26], Chung *et al.* [27], and Hong *et al.* [28] used machine learning algorithms including a deep neural network to classify sleep stages and REM and non-REM sleep.

As explained above, a number of studies have been reported in this active field. Despite this, an accurate signal processing technique for the noncontact measurement of HRV and the LF/HF ratio has not yet been established. In particular, the quantitative measurement of the LF/HF ratio during sleep would be of practical significance, but many recent studies in radar-based noncontact sleep monitoring have focused on the classification of sleep stages. In this paper, we introduce two techniques to improve accuracy in the measurement of the LF/HF ratio using an ultra-wideband (UWB) millimeter-wave (MMW) multiple-input multiple-output (MIMO) array radar system. First, we introduce the maximum ratio combining (MRC) technique, which is an adaptive array processing technique, to improve the signal-to-noise ratio (S/N) of the radar echo. Next, we introduce a reliability index that is the total power of HRV to detect accuracy deterioration. Using the reliability index, we selectively use accurate, continuous HRV estimates to obtain a reliable LF/HF ratio, which would be impossible without the technique introduced in this paper. We verify the effectiveness of these techniques by comparing them with the reference HRV obtained using ECG. By integrating these techniques, the LF/HF ratio of a sleeping person is successfully measured in a noncontact manner using a radar system. Preliminary results of this study were presented in [29]. The difference between [29] and the present paper is that the present paper introduces a reliability index to exclude inaccurate heartbeat estimates, as explained in Section IV-B.

II. System Model and Measurement Setup

In this study, we use a UWB MMW MIMO radar system with a center frequency of 60.5 GHz and bandwidth of 1.25 GHz, which corresponds to a range resolution of 12.0 cm. The system is MIMO array radar that comprises two transmitting and four receiving elements, which results in an 8-channel radar system. Fig. 1 shows a photograph of the radar system and Table I shows its major parameters. Two transmitting elements (Tx1 and Tx2) are vertically arrayed, whereas four receiving elements (Rx1, Rx2, Rx3, and Rx4) are horizontally arrayed, as shown in Fig. 1. The array elements are open-ended waveguide antennas, and they are all vertically polarized. A MIMO array system with

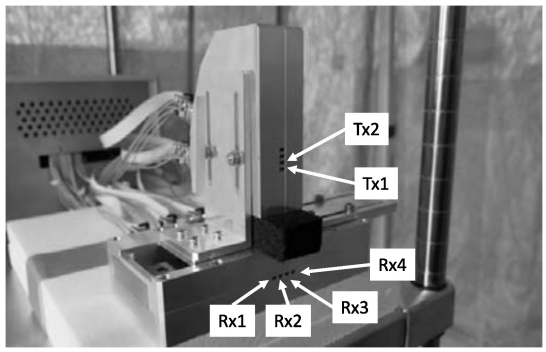

Fig. 1. Ultrawideband MIMO array radar system used in this study.

TABLE I
Radar Parameters

Center frequency	60.5 GHz
Bandwidth	1.25 GHz
output	Under 20.0 mW
Measurement cycle	0.458ms
Beam width	±48 degrees
# of transmit elements	2
# of receive elements	4
Element spacing	4.5 mm
Element size	3.5 mm × 1.7 mm
Modulation	binary phase modulation with m-sequence

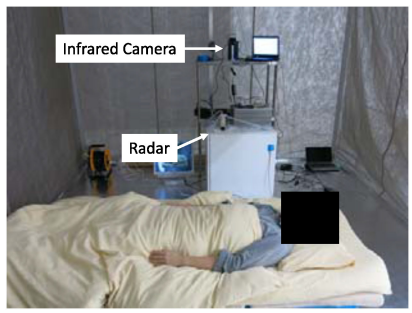

Fig. 2. Measurement setup and a participant in a bed. The cabinet contained an infrared camera and ultra-wideband MIMO array radar. An ECG device was attached to the participant's chest.

N_{T} transmit and N_{R} receive elements can increase the S/N by a factor of the number of channels $N_{\mathrm{T}}N_{\mathrm{R}}$. Because our system has $N_{\mathrm{T}}N_{\mathrm{R}} = 8$ channels, an S/N gain of 9 dB can be expected in an ideal case. Generally, by increasing the number of MIMO channels, a larger S/N gain can be expected, which enables the accurate vital measurement of a person located far from the radar antennas.

Fig. 2 shows the actual measurement setup with a participant. An infrared video camera and the radar system were both installed in a cabinet. Additionally, an ECG device was attached to the chest of the participant during the measurement, which was used as a reference for the heart rate.

We performed measurements overnight so that we could monitor unconscious body movement and heart rate during sleep. Snapshots of the infrared video footage are presented in Fig. 3 ($t = 100$, 173, and 188 s for the top, middle, and bottom

Fig. 3. Video capture images of the sleeping participant rolling over in scenario A. Images were captured at $t = 100$, 173, and 188 s for the top, middle, and bottom photographs, respectively.

photographs, respectively), which shows body motion, including rolling over, and limb motion, both performed unconsciously.

III. Radar and MIMO Signal Processing

A. Measurement of Physiological Displacement

Because millimeter waves can penetrate clothing and blankets, radar systems can measure the skin displacement of a person who is dressed and asleep in a bed. The received signal is down-converted to the intermediate frequency band and quadrature-demodulated to obtain in-phase (I) and quadrature (Q) signals, which results in a complex-valued signal. If there is only a single echo reflected off a single target located at distance $d(t) = d_0 + \Delta d(t)$ from the antennas, then a complex-valued signal for slow time t and fast time τ is approximately expressed as

$$s(t,\tau) = Ap\{\tau - 2d_0/c - 2\Delta d(t)/c\} \cdot \exp\left[\mathrm{j}k\left\{\tau - 2d_0/c - 2\Delta d(t)/c\right\}\right], \quad (1)$$

where A is the amplitude and $p(\tau)$ is the pulse envelope waveform that includes the effect of frequency-dependent scattering, propagation, antennas, amplifiers, and filters. If a target echo is detected approximately at fast time $\tau = 2d_0/c$, then the time-dependent slight displacement component $\Delta d(t)$ can be measured from the phase of $s(t, 2d_0/c)$ because the time-dependent displacement is much smaller than d_0, that is, $|\Delta d(t)| \ll d_0$, and $\Delta d(t)$ does not significantly affect envelope $p(\tau - 2d_0/c - 2\Delta d(t)/c) \simeq p(\tau - 2d_0/c)$. Therefore, signal phase $\angle s(t,\tau)$ is converted to a displacement as $\Delta d(t) \simeq \lambda \angle s(t,\tau)/4\pi$ and processed to estimate the heart rate of the person under test. When there is only a single dominant echo, received signal s_{rec} is written as $s_{\mathrm{rec}}(t,\tau) = s(t,\tau) + u(\tau) + n(t,\tau)$, where u is static clutter and n is noise. Next, a circle fitting technique is used [30] to reject static clutter. Hu's method [19] is one of the most accurate circle fitting methods [30]. Hu's method estimates static clutter u by solving an optimization problem $u = \arg\min_{u'} \epsilon(u')$, where $\epsilon(u') = \sum_{i=1}^{L}(|s_{\mathrm{rec}}(t_i) - u'| - A_0(u'))^2$, τ is omitted for simplicity, L is the number of data samples, and $A_0(u')$ is determined by $A_0(u')^2 = \sum_{i=1}^{L} |s_{\mathrm{rec}}(t_i) - u'|^2/L$. Static clutter is then subtracted to obtain clutter-free signal $s_0 = s_{\mathrm{rec}} - u$. Finally, phase $\angle s_0(t,\tau)$ is processed using the topology method [31], which is one of the most accurate algorithms, to estimate the heart interbeat interval (IBI) $h(t)$, which is the reciprocal of the instantaneous heart rate. In the topology method, six types of features are extracted from phase waveform $\angle s_0(t,\tau)$, and the heartbeat IBI is accurately estimated using the topological similarity of the feature sequence patterns of the waveform [31].

B. MIMO Array Radar Signal Processing

During the measurement, the participant was asleep in a bed and prone to unconscious movement, such as rolling over, which resulted in the body position varying over time. Because of the changing position, we formed the array beam pattern using adaptive array signal processing with the MIMO system so that a high S/N was maintained throughout the measurement. The MIMO array antenna consisted of two transmitting and four receiving elements, and $2 \times 4 = 8$ channels were obtained in total. We used the MRC technique, which is an adaptive array signal processing algorithm in the field of telecommunications, because the technique maximizes the output power even when the element phases are not calibrated.

The received 8-channel signals are denoted by signal vector $\boldsymbol{s}(t) = [s_{1,1}, s_{1,2}, \ldots, s_{2,4}]^{\mathrm{T}}$, where superscript T is a transpose operator and $s_{i,j}$ is the signal for the i-th transmitting and j-th receiving elements. The correlation matrix is expressed as

$$R_{ss} = \langle \boldsymbol{s}(t)\boldsymbol{s}^{\mathrm{H}}(t) \rangle \simeq \int \boldsymbol{s}(t)\boldsymbol{s}^{\mathrm{H}}(t)\mathrm{d}t, \quad (2)$$

where superscript H is a complex-conjugate transpose operator and $\langle\rangle$ is an expectation operator achieved using ensemble averaging, which can be approximated using the time average.

By applying the eigenvalue decomposition of R_{ss}, we obtain

$$R_{ss} = [\boldsymbol{v}_1\boldsymbol{v}_2\cdots\boldsymbol{v}_N]\mathrm{diag}\{\sigma_1,\sigma_2,\ldots,\sigma_N\}[\boldsymbol{v}_1\boldsymbol{v}_2\cdots\boldsymbol{v}_N]^{\mathrm{H}}, \quad (3)$$

where $\sigma_1, \sigma_2, \ldots, \sigma_N$ are eigenvalues sorted in descending order, and eigenvector $\boldsymbol{v}_i$ $(i = 1, \ldots, N)$ corresponds to the i-th eigenvalue σ_i. The dimension of the vectors is denoted by $N = 8$. The MRC technique uses the first eigenvector $\boldsymbol{v}_1$ as weight vector $\boldsymbol{w} = \boldsymbol{v}_1$ and obtains output signal $s(t)$ as $s(t) = \boldsymbol{w}^H\boldsymbol{s}(t) = \boldsymbol{v}_1^H\boldsymbol{s}(t)$, where the eigenvectors and weight vector are normalized, that is, $|\boldsymbol{v}_i|^2 = 1$ for $i = 1, 2, \ldots, N$ and $|\boldsymbol{w}|^2 = 1$. If only a single echo is received, the MRC technique provides a weight that maximizes the S/N, which corresponds to the matched filter.

IV. Heart Rate Variability and Reliability

A. Heart Rate Variability and Nervous Systems

Activity in the autonomic nervous system can be estimated from the time-dependent heart rate called HRV. Therefore, mental stress, for example, can be inferred from the measurement of HRV. When the sympathetic nervous system, which is associated with mental stress, is activated, the LF component ($f_1 \leq f \leq f_2$) increases, whereas the activation of the parasympathetic nervous system is identified by the intensity of the HF component ($f_2 \leq f \leq f_3$), where $f_1 = 0.04$ Hz, $f_2 = 0.15$ Hz, and $f_3 = 0.4$ Hz. Therefore, mental stress can be detected using LF/HF ratio ρ expressed as

$$\rho(t) = \frac{\int_{f_1}^{f_2} S_{\mathrm{HR}}(t,f)\mathrm{d}f}{\int_{f_2}^{f_3} S_{\mathrm{HR}}(t,f)\mathrm{d}f}, \tag{4}$$

where $S_{\mathrm{HR}}(t,f)$ is a spectrogram of HRV expressed as a function of slow time t and frequency f. LF/HF ratio $\rho(t)$ is widely used as an index that indicates the autonomic nervous system balance.

B. Heart Rate Variability and Reliability

As mentioned in the previous section, the frequency analysis of HRV reveals the mental state of the person under test. To obtain a frequency spectrum, however, we require an HRV time series that is continuously accurate over a time period that is greater than the reciprocal of the lower cut-off frequency of the LF, $1/f_1 = 25$ s, which cannot always be satisfied in the noncontact measurement of HRV. Therefore, it is necessary to automatically estimate the reliability of the measured HRV.

In this section, we propose using the total power of non-direct-current (non-DC) components of the HRV time series. This technique is based on a hypothesis, which is that the reliable HRV time series has a moderate non-DC component, which is formulated as

$$U_{\mathrm{HR}} = \sqrt{\int_{f_1}^{f_4} S_{\mathrm{HR}}(f)\mathrm{d}f}, \tag{5}$$

where $U_{\mathrm{HR}}(t)$ is an unreliability index. The lower-cutoff frequency $f_1 = 0.04$ Hz is the same as the lower-cutoff frequency f_1 of the LF. The higher-cutoff frequency $f_4 = 2.48$ Hz is the Nyquist frequency determined by the sampling frequency. If f_1 is set too low, then physiologically meaningless components are included in the results, whereas if f_1 is set too high, then physiologically important HRV is erroneously excluded. Large U_{HR} suggests that the estimated HRV is unlikely to be accurate. The reciprocal of U_{HR} is also introduced as $R_{\mathrm{HR}} = 1/U_{\mathrm{HR}}$, which denotes a reliability index.

These reliability and unreliability indices are defined as follows: Generally, we can observe HRV because of the activity level of the sympathetic/parasympathetic nervous systems. However, there is a physiological limitation to actual heart rate change over time. Excessive change in heart rate is considered to indicate the incorrect measurement of heart rate; an incorrect heart rate would look like random white noise that is uniformly distributed over a wide frequency band, which is detected and converted to R_{HR} and U_{HR} introduced above.

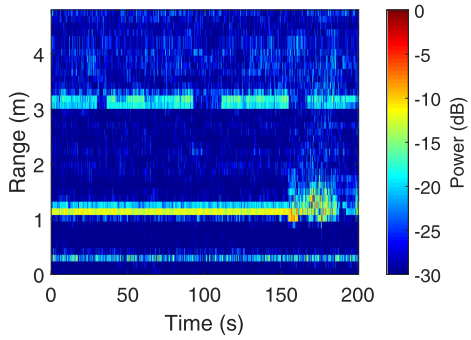

Fig. 4. Signal intensity for a slow time and range for scenario A.

V. Performance Evaluation of the Proposed Techniques

A. Measurement Scenarios

We evaluated the performance of the proposed techniques by applying them to two scenarios: A and B. The measurement time of each scenario was 200 s. In scenario A, the participant remained stationary for $t < 160$ s, and started to move and roll over at $t \simeq 160$ s and $t \simeq 170$ s (see Fig. 4). In scenario B, the participant remained stationary except for 65 s $< t <$ 85 s. Fig. 4 shows signal intensity $|s(t,\tau)|^2$ as a function of slow time t and range $r = c\tau/2$ for scenario A. We observe that the echo from the participant remained at almost the same range around $r =$ 1.1 m until the body movement that occurred at $t = 160$ s. We also observe a time-varying echo caused by body motion for 160 s $< t <$ 180 s. The weaker echo at around $r \simeq 3.2$ m was caused by the reflection from the wall.

B. Evaluation of MIMO Array Signal Processing

Next, we evaluated the performance of the MRC array signal processing that was introduced in Section III. The upper graph of Fig. 5 shows the S/N for scenario A as a function of slow time t. The red, yellow, and purple lines show the maximum, minimum, and average S/N, respectively, whereas the blue line shows the S/N of the combined multi-channel signal $s(t)$ using the MRC technique. From this figure, we observe that the MRC improved the S/N by 8 dB from the average, and 6 dB from the best single channel. This result suggests that the MRC is effective for improving the S/N, which is necessary for measuring slight skin displacement caused by the heartbeat.

The lower graph in Fig. 5 shows the heart rate sequences estimated using the ECG (black line), a single radar channel with the maximum power (red circles), and the multiple radar channels combined using the MRC (blue plots). The root-mean-square (RMS) error in measuring the heartbeat IBI was 182 ms using the best single channel and 148 ms using multiple channels combined using the MRC technique, which resulted in an 18% improvement. Please note that the RMS errors were calculated from the entire time period of 200 s. This result suggests the

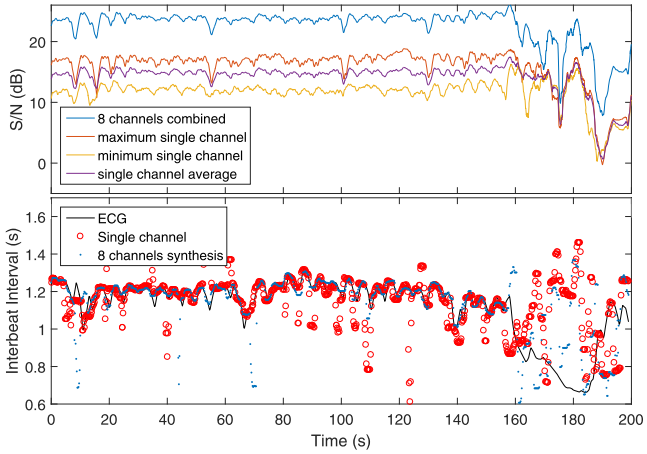

Fig. 5. S/N of the maximum, minimum, and average single channels and all multiple channels combined using MRC (upper figure) and the IBI measured using the ECG and the maximum-power single channel and multiple channels combined using MRC (lower figure).

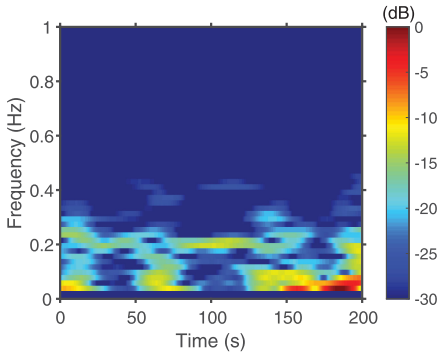

Fig. 6. Spectrogram of the IBI measured using ECG for scenario A.

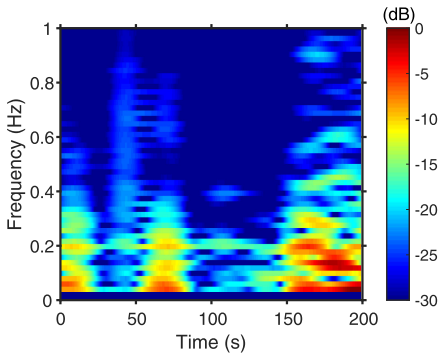

Fig. 7. Spectrogram of the IBI measured using radar for scenario A.

effectiveness of the MRC technique in improving the heart rate measurement accuracy. However, the accuracy significantly degraded for $t > 160$ s because of body motion.

C. Evaluation of the Reliability Index

We investigate the performance of the proposed reliability index. Figs. 6 and 7 show spectrograms of IBIs measured using the ECG and radar for scenario A. We observe a similarity

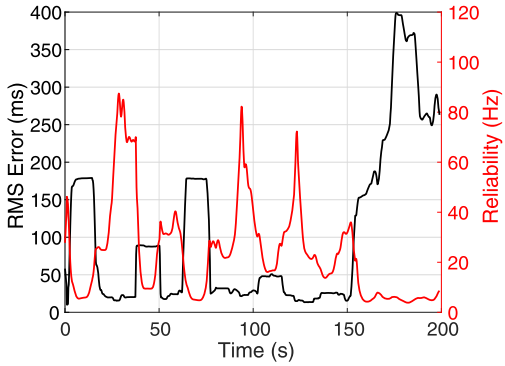

Fig. 8. RMS error in estimating the IBI (black line) and the proposed reliability index $R_{\mathrm{HR}}(t)$ (red line) for scenario A. The RMS error is relatively small when $R_{\mathrm{HR}}(t)$ is large.

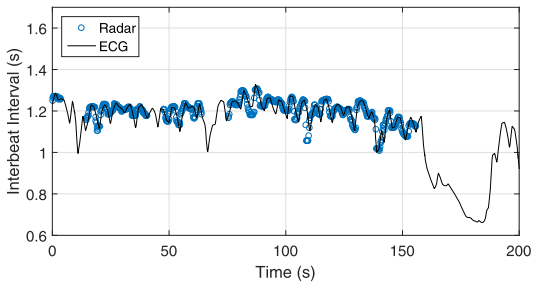

Fig. 9. Heartbeat IBI measured using ECG (black line) and radar (blue circles) using the proposed method (scenario A). The IBI plots are displayed only if the reliability index is higher than threshold $R_{\mathrm{HR}}(t) > R_{\mathrm{th}}$.

between these spectrograms for 90 s $< t <$ 160 s before significant body movement starts at $t = 160$ s. By contrast, when the participant is in motion ($t \geq 160$ s), we observe a nonnegligible discrepancy between the two spectrograms. During body motion, the intensity of the non-DC component of the radar-based IBI spectrogram increases over a wide frequency range, which is exploited as a reliability index in the proposed approach.

Fig. 8 shows a time variation of the RMS error $e_{\mathrm{v}}(t)$ and reliability $R_{\mathrm{HR}}(t)$, where $e_{\mathrm{v}}(t)$ is calculated as

$$e_{\mathrm{v}}(t) = \sqrt{\frac{\sum_{i=1}^{I} w(t_i - t)|h_{\mathrm{r}}(t_i) - h_{\mathrm{E}}(t_i)|^2}{\sum_{i=1}^{I} w(t_i - t)}}, \tag{6}$$

where I is the number of IBI samples, h_{r} and h_{E} are heartbeat IBIs estimated using the radar and ECG, respectively, and $w(\cdot)$ is a Tukey window with a length of 12.8 s and taper parameter of 0.7. From this figure, we observe that $R_{\mathrm{HR}}(t)$ is low for $t \geq$ 90 s and 160 s $\geq t$, which is consistent with the time when the RMS error is also large. The large RMS error is the reason for the discrepancy between Figs. 6 and 7. We confirmed that there is a positive correlation between the RMS error and unreliability index $U_{\mathrm{HR}} = 1/R_{\mathrm{HR}}$ with a correlation coefficient of 0.88. This result indicates that reliability index $R_{\mathrm{HR}}(t)$ is a good indicator of accuracy for the measurement of the heartbeat. Fig. 9 shows the IBIs measured using radar (blue circles) and ECG (black line), where the radar IBI is not displayed if the reliability is lower than a threshold ($R_{\mathrm{HR}}(t) < R_{\mathrm{th}}$), where $R_{\mathrm{th}} = 12.5$ Hz. As shown in the figure, almost all low-accuracy IBI plots were

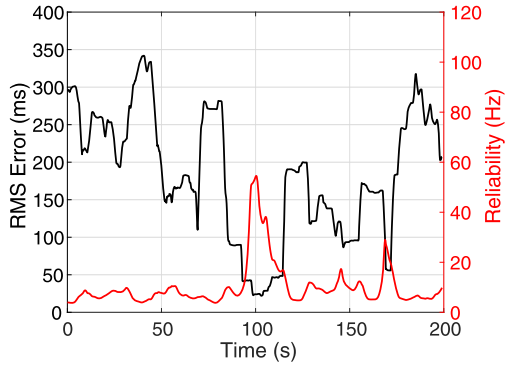

Fig. 10. RMS error in estimating the IBI (black line) and the proposed reliability index $R_{\mathrm{HR}}(t)$ (red line) for scenario B. The RMS error is small when $R_{\mathrm{HR}}(t)$ is large.

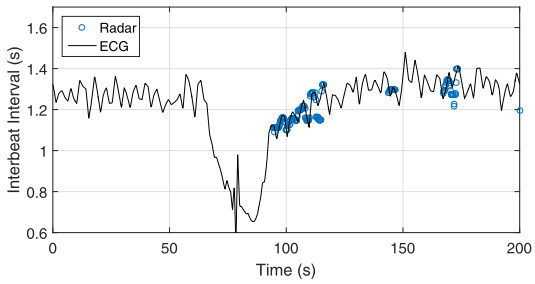

Fig. 11. Heartbeat IBI measured using ECG (black line) and radar (blue circles) using the proposed method (scenario B). The IBI plots are displayed only if the reliability index is high $R_{\mathrm{HR}}(t) > R_{\mathrm{th}}$.

removed successfully. Thus, the proposed reliability index is effective for distinguishing reliable and unreliable IBI estimates.

The use of the reliability index achieved an RMS error of 23.4 ms (Fig. 9), where RMS error e was calculated using IBI samples whose reliability was greater than the threshold as

$$e = \sqrt{\frac{\sum_{i=1}^{I} H(R_{\mathrm{HR}}(t_i) - R_{\mathrm{th}})|h_{\mathrm{r}}(t_i) - h_{\mathrm{E}}(t_i)|^2}{\sum_{i=1}^{I} H(R_{\mathrm{HR}}(t_i) - R_{\mathrm{th}})}}, \quad (7)$$

where $H(\cdot)$ is a unit step function. The original RMS error was 148 ms (Fig. 5), which suggests an improvement of 6.3 times. Although several IBI estimate points disappeared, which resulted in a great deal of missing data, the measurement of the LF/HF ratio requires accurate IBI estimates rather than a large number of data points that include unreliable estimates.

Next, the same techniques were applied to scenario B. Reliability index $R_{\mathrm{HR}}(t)$ and the RMS error are shown in Fig. 10. Except for $t \simeq 100$ s, the reliability was low, which is consistent with the large RMS error. In scenario B, the correlation coefficient between unreliability index $U_{\mathrm{HR}} = 1/R_{\mathrm{HR}}$ and the RMS was 0.80, which is not as high as that in scenario A. Despite this, the reliability index provides useful information for interpreting the IBI values measured using radar.

Fig. 11 shows the IBI measured using the ECG (black line) and radar (blue circles), where the radar estimates are displayed only if the reliability index is larger than a threshold ($R_{\mathrm{HR}}(t) > R_{\mathrm{th}}$), where $R_{\mathrm{th}} = 12.5$ Hz. Although an accurate heart rate was measured using radar only for a short time, the accuracy

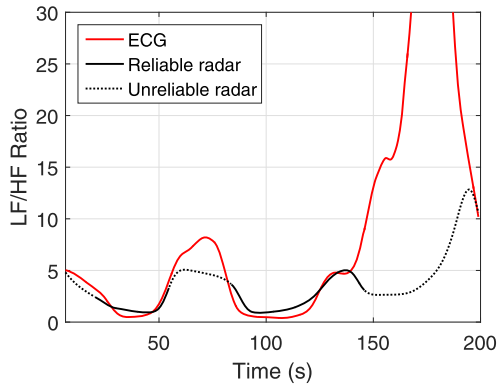

Fig. 12. Mental stress index $\rho(t)$ for scenario A.

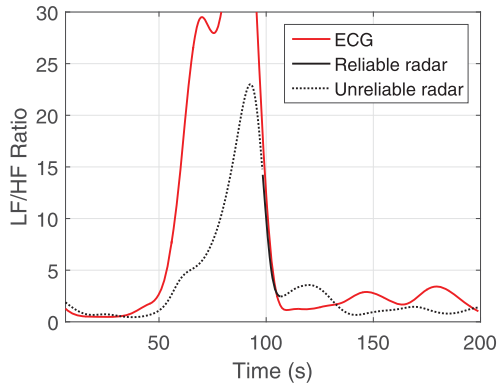

Fig. 13. Mental stress index $\rho(t)$ for scenario B.

is sufficient. In this case, the RMS error using the proposed reliability index was 28.3 ms. Compared with the original RMS error of 205.0 ms without using the reliability index, the accuracy improved by 7.2 times using the proposed reliability index.

D. Estimation of the LF/HF Ratio

In this section, we investigate whether ECG and radar measurements can provide a consistent LF/HF ratio. Fig. 12 shows the LF/HF ratio calculated from ECG data (red line) and also from radar data (black line) in scenario A, where the solid and dashed black lines indicate the estimates for the reliability index higher and lower than threshold $R_{\mathrm{HR}}(t) < R_{\mathrm{th}}$ ($R_{\mathrm{th}} = 12.5$ Hz), respectively. In the figure, we observe that the estimates from ECG and radar are consistent when the reliability is high, whereas there is a discrepancy between them when the reliability is low, which indicates the effectiveness of the proposed reliability index. The original correlation coefficient between the estimates from the ECG and radar was 0.38, whereas the correlation coefficient was 0.87 only when the reliability was above the threshold, which means that the proposed reliability index increased the correlation coefficient.

Fig. 13 shows the same comparison for scenario B. In this case, the reliability is larger than the threshold within a limited time, where the radar-based estimate is a solid black line. The correlation coefficient between the ECG and radar estimates was 0.89 without the reliability index and 0.99 with the reliability

index. These results indicate the importance of the proposed reliability index in measuring the LF/HF ratio using a radar system.

VI. Discussion

A. Selection of the Frequency Band

An operating frequency band is one of the most important parameters in radar-based heartbeat monitoring. For example, many recent studies use low-frequency CW radar at 2.4–2.5 GHz [21], [28], [32]–[34], 4.8 GHz [33], and 5.8 GHz [23], [35]–[36], and sub-MMW CW at 24 GHz [37]–[38], whereas some use UWB radar at 4.2 GHz [39]–[41], 6.8 GHz [42], 15 GHz [43], 24 GHz [36], 77 GHz [44], and 122 GHz [45].

In this study, we used a UWB radar system with a bandwidth of 1.25 GHz, which corresponds to a high range resolution of 12.0 cm, which can distinguish most echoes from body parts, in addition to other clutter, thus enabling the accurate measurement of the heartbeat. Because of radio spectrum allocation regulation, however, the use of UWB radar is allowed only in specific frequency bands (e.g., 24, 60, 77, and 79 GHz). In particular, MMW bands 60, 77, and 79 GHz are sensitive to a small displacement, and thus, can measure the heartbeat accurately. Additionally, unlike 77 and 79 GHz bands, 60-GHz systems suffer relatively less interference from automotive radar systems. For these reasons, we selected the 60 GHz band in our study. Despite this, the proposed techniques in the present paper can be applied equally well to lower-frequency UWB radar, provided the system's phase jitter is small. Note that low-frequency array radar systems are physically large and bulky, which can be disadvantageous in practice.

B. Selection of the Reliability Threshold

In this study, reliability threshold $R_{\rm th} = 12.5$ Hz was selected empirically. If threshold $R_{\rm th}$ is to be optimized for a specific target person, then the value depends on the physiological characteristics of that person. If the target person's natural heart rate fluctuation is large, then threshold $R_{\rm th}$ should be also set to a large value to avoid mislabeling. If the same threshold value $R_{\rm th}$ is to be used for multiple people, then the value should be set based on the average heart rate fluctuation across the subjects of a clinical study.

In this study, only one participant and two three-minute data were used to evaluate the proposed algorithm. The next step of this study requires the measurement of a large number of participants so that the effectiveness of the proposed techniques can be evaluated statistically. Such a large-scale measurement would also help to tune important parameters, such as the reliability threshold, that were set empirically in this study.

VII. Conclusion

In this paper, we introduced techniques necessary for the accurate noncontact measurement of the heartbeat during sleep using ultra-wideband array radar. First, we introduced a MIMO signal processing technique to improve the S/N, which was demonstrated to be able to improve the accuracy in estimating the IBI. We then proposed a reliability index, which is the reciprocal of the intensity of the non-DC component of the IBI time series. The index was demonstrated to be effective for detecting unreliable IBI estimates from radar data. The techniques introduced in the present paper are key technology for applying radar-based noncontact vital measurement to sleep monitoring and assessing the LF/HF ratio, which is an index of autonomic nervous system activities.

Acknowledgment

The authors would like to thank Prof. T. Sato of Kyoto University, Dr. S. Okumura of MaRI Co., Ltd., K. Inoue, T. Fukuda, K. Mizutani, H. Sakai of Panasonic Corp., and K. Watanabe of Denso Ten Technology, Ltd., for their help with this study, and also M. Garcia, Ph.D., from Edanz Group for editing a draft of this manuscript.

References

[1] M. Pagani *et al.*, "Power spectral analysis of heart rate and arterial pressure variabilities as a marker of sympatho-vagal interaction in man and conscious dog," *Circulation Res.*, vol. 59, no. 2, pp. 178–193, Aug. 1986.

[2] A. Malliani, M. Pagani, F. Lombardi, and S. Cerutti, "Cardiovascular neural regulation explored in the frequency domain," *Circulation*, vol. 84, no. 2, pp. 482–492, Aug. 1991.

[3] G. G. Berntson *et al.*, "Heart rate variability: Origins, methods, and interpretive caveats," *Psychophysiology*, vol. 34, no. 6, pp. 623–648, Nov. 1997.

[4] G. B. Stanley, K. Poolla, and R. A. Siegel, "Threshold modeling of autonomic control of heart rate variability," *IEEE Trans. Biomed. Eng.*, vol. 47, no. 9, pp. 1147–1153, Sep. 2000.

[5] J. Mateo and P. Laguna, "Improved heart rate variability signal analysis from the beat occurrence times according to the IPFM model," *IEEE Trans. Biomed. Eng.*, vol. 47, no. 8, pp. 985–996, Aug. 2000.

[6] M. A. Garcia-Gonzalez and R. Pallas-Areny, "A novel robust index to assess beat-to-beat variability in heart rate time-series analysis," *IEEE Trans. Biomed. Eng.*, vol. 48, no. 6, pp. 617–621, Jun. 2001.

[7] R. J. Leor-Librach, S. Eliash, E. Kaplinsky, and B.-Z. Bobrovsky, "Very low-frequency heart rate variability wave amplitude and sympathetic stimulation—Characterization and modeling," *IEEE Trans. Biomed. Eng.*, vol. 50, no. 7, pp. 797–803, Jul. 2003.

[8] S. Sarkar and J. Koehler, "A dynamic risk score to identify increased risk for heart failure decompensation," *IEEE Trans. Biomed. Eng.*, vol. 60, no. 1, pp. 147–150, Jan. 2013.

[9] M. Ako *et al.*, "Correlation between electroencephalography and heat rate variability during sleep," *Psych. Clin. Neurosci.*, vol. 57, pp. 59–65, Feb. 2003.

[10] B. Knorr, M. Akay, and T. A. Mellman, "Heart rate variability during sleep and the development of PTSD following traumatic injury," in *Proc. Annu. Int. Conf. IEEE Eng. Med. Biol. Soc.*, 2003, pp. 354–357.

[11] T. A. Mellman, B. R. Knorr, W. R. Pigeon, J. C. Leiter, and M. Akay, "Heart rate variability during sleep and the early development of posttraumatic stress disorder," *Biol. Psych.*, vol. 55, no. 9, pp. 953–956, May 2004.

[12] A. Kishi, B. H. Natelson, F. Togo, Z. R. Struzik, D. M.Rapoport, and Y. Yamamoto, "Sleep stage transitions in chronic fatigue syndrome patients with or without fibromyalgia," in *Proc. 32nd Annu. Int. Conf. IEEE Eng. Med. Biol. Soc.*, 2010, pp. 5391–5394.

[13] G. Milicević, "Low to high frequency ratio of heart rate variability spectra fails to describe sympatho-vagal balance in cardiac patients," *Collegium Antropologicum*, vol. 29, pp. 295–300, Jun. 2005.

[14] G. E. Billman, "The LF/HF ratio does not accurately measure cardiac sympatho-vagal balance," *Frontiers Physiol.*, vol. 4, no. 26, pp. 1–5, Feb. 2013.

[15] W. V. Rosenberg, T. Chanwimalueang, T. Adjei, U. Jaffer, V. Goverdovsky, and D. P. Mandic, "Resolving ambiguities in the LF/HF ratio: LF-HF scatter plots for the categorization of mental and physical stress from HRV," *Frontiers Physiol.*, vol. 8, pp. 1–12, Jun. 2017.

[16] Y. Zhu, X. Yang, Z. Wang, and Y. Peng, "An evaluating method for autonomic nerve activity by means of estimating the consistency of heart rate variability and QT variability," *IEEE Trans. Biomed. Eng.*, vol. 61, no. 3, pp. 938–945, Mar. 2014.
[17] M. Nardelli, G. Valenza, A. Greco, A. Lanata, and E. P. Scilingo, "Recognizing emotions induced by affective sounds through heart rate variability," *IEEE Trans. Affect. Comput.*, vol. 6, no. 4, pp. 385–394, Oct.–Dec. 2015.
[18] D. P. Tobón, S. Jayaraman, and T. H. Falk, "Spectro-temporal electrocardiogram analysis for noise-robust heart rate and heart rate variability measurement," *IEEE J. Trans. Eng. Health Med.*, vol. 5, 2017, Art. no. 1900611, doi: 10.1109/JTEHM.2017.2767603.
[19] W. Hu, Z. Zhao, Y. Wang, H. Zhang, and F. Lin, "Noncontact accurate measurement of cardiopulmonary activity using a compact quadrature Doppler radar sensor," *IEEE Trans. Biomed. Eng.*, vol. 61, no. 3, pp. 725–735, Mar. 2014.
[20] D. Nagae and A. Mase, "Measurement of heart rate variability and stress evaluation by using microwave reflectometric vital signal sensing," *Rev. Sci. Instrum.*, vol. 81, 2010, Art. no. 094301.
[21] M. Nosrati and N. Tavassolian, "High-accuracy heart rate variability monitoring using Doppler radar based on Gaussian pulse train modeling and FTPR algorithm," *IEEE Trans. Microw. Theory Techn.*, vol. 66, no. 1, pp. 556–567, Jan. 2018.
[22] E. Mogi and T. Ohtsuki, "Heartbeat detection with Doppler radar based on estimation of average R-R interval using Viterbi algorithm," in *Proc. IEEE 27th Int. Symp. Pers., Indoor, Mobile Radio Commun.*, Valencia, 2016, pp. 1–5.
[23] M. Li and J. Lin, "Wavelet-transform-based data-length-variation technique for fast heart rate detection using 5.8-GHz CW Doppler radar," *IEEE Trans. Microw. Theory Techn.*, vol. 66, no. 1, pp. 568–576, Jan. 2018.
[24] M. Baboli, A. Singh, B. Soll, O. Boric-Lubecke, and V. M. Lubecke, "Good night: Sleep monitoring using a physiological radar monitoring system integrated with a polysomnography system," *IEEE Microw. Mag.*, vol. 16, no. 6, pp. 34–41, Jul. 2015.
[25] F. Lin *et al.*, "SleepSense: A noncontact and cost-effective sleep monitoring system," *IEEE Trans. Biomed. Circuits Syst.*, vol. 11, no. 1, pp. 189–202, Feb. 2017.
[26] L. Zhang, J. Xiong, H. Zhao, H. Hong, X. Hu, and C. Li, "Sleep stages classification by CW Doppler radar using bagged trees algorithm," in *Proc. IEEE Radar Conf.*, 2017, pp. 788–791.
[27] K.-Y. Chung, K. Song, S. H. Cho, and J.-H. Chang, "Noncontact sleep study based on an ensemble of deep neural network and random forests," *IEEE Sensors J.*, vol. 18, no. 17, pp. 7315–7324, Sep. 2018.
[28] H. Hong, L. Zhang, C. Gu, Y. Li, G. Zhoug, and X. Zhu, "Noncontact sleep stage estimation using a CW Doppler radar," *IEEE Trans. Emerg. Sel. Topics Circuits Syst.*, vol. 8, no. 2, pp. 260–270, Jun. 2018.
[29] T. Sakamoto, "Noncontact measurement of human vital signs during sleep using low-power millimeter-wave ultrawideband MIMO array radar," in *Proc. IEEE Int. Microw. Biomed. Conf.*, Nanjing, China, 2019, pp. 168–171.
[30] S. Okumura *et al.*, "Comparison of clutter rejection techniques for measurement of small displacements of body surface using radar," *Electron. Lett.*, vol. 52, no. 19, pp. 1635–1637, Sep. 2016.
[31] T. Sakamoto *et al.*, "Feature-based correlation and topological similarity for interbeat interval estimation using ultrawideband radar," *IEEE Trans. Biomed. Eng.*, vol. 63, no. 4, pp. 747–757, Apr. 2016.
[32] Z.-P. Yang and Y.-C. Chiang, "Vital signal radar with adaptive compensation circuits to effectively eliminate DC offsets," *IEEE Microw. Wireless Compon. Lett.*, vol. 28, no. 1, pp. 88–90, Jan. 2018.
[33] F. Zhu, K. Wang, and K. Wu, "A fundamental-and-harmonic dual-frequency Doppler radar system for vital signs detection enabling radar movement self-cancellation," *IEEE Trans. Microw. Theory Techn.*, vol. 66, no. 11, pp. 5106–5118, Nov. 2018.
[34] C. Gu, Y. He, and J. Zhu, "Noncontact vital sensing with a miniaturized 2.4 GHz circularly polarized Doppler radar," *IEEE Sens. Lett.*, vol. 3, no. 7, Jul. 2019, Art. no. 3501204. [Online]. Available: http://dx.doi.org/10.1109/LSENS.2019.2924695
[35] M. Mercuri *et al.*, "A direct phase-tracking Doppler radar using wavelet independent component analysis for non-contact respiratory and heart rate monitoring," *IEEE Trans. Biomed. Circuits Syst.*, vol. 12, no. 3, pp. 632–643, Jun. 2018.
[36] Q. Lv *et al.*, "Doppler vital signs detection in the presence of large-scale random body movements," *IEEE Trans. Microw. Theory Techn.*, vol. 66, no. 9, pp. 4261–4270, Sep. 2018.
[37] C. Ye, K. Toyoda, and T. Ohtsuki, "A stochastic gradient approach for robust heartbeat detection with Doppler radar using time-window-variation technique," *IEEE Trans. Biomed. Eng.*, vol. 66, no. 6, pp. 1730–1741, Jun. 2019.
[38] V. L. Petrović, M. M. Janković, A. V. Lupšić, V. R. Mihajlović, and J. S. Popović-Božović, "High-accuracy real-time monitoring of heart rate variability using 24 GHz continuous-wave Doppler radar," *IEEE Access*, vol. 7, pp. 74721–74733, 2019.
[39] H. Shen *et al.*, "Respiration and heartbeat rates measurement based on autocorrelation using IR-UWB radar," *IEEE Trans. Circuits Syst. II, Express Briefs*, vol. 65, no. 10, pp. 1470–1474, Oct. 2018.
[40] K.-K. Shyu, L.-J. Chiu, P.-L. Lee, T.-H. Tung, and S.-H. Yang, "Detection of breathing and heart rates in UWB radar sensor data using FVPIEF-based two-layer EEMD," *IEEE Sensors J.*, vol. 19, no. 2, pp. 774–784, Jan. 2019.
[41] Z. Duan and J. Liang, "Non-contact detection of vital signs using a UWB radar sensor," *IEEE Access*, vol. 7, pp. 36888–36895, 2019.
[42] H.-S. Cho, B. Choi, and Y.-J. Park, "Monitoring heart activity using ultra-wideband radar," *Electron. Lett.*, vol. 55, no. 16, pp. 878–881, 2019. [Online]. Available: http://dx.doi.org/10.1049/el.2019.1438
[43] T.-H. Liu, M.-L. Hsu, and Z.-M. Tsai, "High ranging accuracy and wide detection range interferometry based on frequency-sweeping technique with vital sign sensing function," *IEEE Trans. Microw. Theory Techn.*, vol. 66, no. 9, pp. 4242–4251, Sep. 2018.
[44] J. Wei, L. Zhang, and H. Liu, "Non-contact life signal extraction and reconstruction technique based on MAE," *IEEE Access*, vol. 7, pp. 110826–110834, 2019.
[45] A. Prat, S. Blanch, A. Aguasca, J. Romeu, and A. Broquetas, "Collimated beam FMCW radar for vital sign patient monitoring," *IEEE Trans. Antennas Propag.*, vol. 67, no. 8, pp. 5073–5080, Aug. 2019.

Takuya Sakamoto (M'04–SM'17) received the B.E. degree in electrical and electronic engineering from Kyoto University, Kyoto, Japan, in 2000 and the M.I. and Ph.D. degrees in communications and computer engineering from the Graduate School of Informatics, Kyoto University, Kyoto, Japan, in 2002 and 2005, respectively.

From 2006 to 2015, he was an Assistant Professor with the Graduate School of Informatics, Kyoto University. From 2011 to 2013, he was a Visiting Researcher with Delft University of Technology, Delft, The Netherlands. In 2017, he was a Visiting Scholar with the University of Hawaii at Manoa, Honolulu, HI, USA. He is currently an Associate Professor with the Graduate School of Engineering, Kyoto University.

Dr. Sakamoto was the recipient of the Masao Horiba Award in 2016. In 2017, he was invited to be a semi-plenary speaker at EuCAP2017 in Paris, France.

Kosuke Yamashita received the B.E. degree in engineering from the University of Hyogo, Himeji, Japan, in 2017, and the M.E. degree in electronics and computer science from the Graduate School of Engineering, University of Hyogo, Himeji, Japan, in 2019. He is currently with Denso Ten, Ltd., Kobe, Japan.